ACCEPTED MANUSCRIPT

Effects of fin arrangement on the melting process in a vertical double-tube heat exchanger considering intermittent boundary conditions

Ali Mehrannia[1], Mohammad Taghilou[2,*]

[1] Master graduate, Department of mechanical engineering, university of Zanjan, Zanjan, Iran
[2] Associate Professor, Department of mechanical engineering, university of Zanjan, Zanjan, Iran
[*]Corresponding author: taghilou@znu.ac.ir

Abstract:

This paper presents a numerical analysis of the solid-liquid phase change within a vertical double-tube heat exchanger containing a phase change material, considering intermittent boundary conditions with application of enthalpy-porosity technique. To enhance the rate of heat transfer, copper fins are integrated on the inner wall of the heat exchanger in both uniform and non-uniform arrangements. While the uniform placement of fins at equal intervals accelerates the melting process, it leads to a portion of the phase change material remaining solid at the bottom of the heat exchanger due to weakened natural convection. Conversely, positioning a greater number of fins with a non-uniform distribution at the bottom of the heat exchanger expedites the overall melting process. It is observed that compared to a finless heat exchanger and under constant boundary temperature, the complete melting time is reduced by 53%, 69%, and 75% for uniform fin distribution, and fin distribution with geometric progression q=2 and q=3, respectively. Furthermore, the findings showed that natural convection leads to a greater increase in liquid fraction during melting compared to the assumption of pure conduction. Specifically, liquid fraction increases by about 40% with natural convection and around 15% with pure conduction during the first melting period. While the decrease in liquid fraction is almost equivalent for both conditions during freezing.

Keywords:

Vertical double-tube heat exchanger, Phase change material, Non-uniform fin distribution, Intermittent boundary condition.

1- **Introduction**

Today, the scientific and engineering communities are increasingly interested in renewable energies as a potential substitute for fossil fuels due to their minimal emission of polluting gases. However, the intermittent and time-sensitive nature of renewable energies has prompted the development of energy storage technologies, particularly latent heat thermal storage (LHTS) systems. One effective method of thermal energy storage involves the use of phase change materials (PCMs) with high energy storage density and the ability to maintain nearly constant temperatures [1, 2]. Nevertheless, this approach comes with challenges such as high cost, low thermal conductivity, and unstable thermophysical properties [3, 4]. Various techniques are employed to address the low thermal conductivity of PCMs, such as adding fins to the storage unit, incorporating nanoparticles with high thermal conductivity, and utilizing PCM within a porous metal medium [5-7].

The configuration, arrangement, and size of the fins significantly impact the flow dynamics and heat transfer within heat exchangers [8]. Additionally, strategies like downward movement of the inner tube in a double-pipe heat exchanger can enhance natural convection and reduce melting time in a horizontal LHTS system [9]. Mahdi et al. [10] have explored the positioning of PCM within heat exchangers, finding that placing PCM in the inner tube rather than the annular space significantly reduces melting time. A comprehensive storage density evaluation (CSDE) criterion has been proposed by Xu et al. [11] as a means to optimize the design of horizontal shell-and-tube heat exchangers with metal fins. Patel et al. [12] have also investigated the use of fins to improve melting and solidification processes within horizontal triplex-tube heat exchangers, with findings indicating that fins are more effective for melting than for freezing, particularly when placed in the lower half of the heat exchanger.

Additionally, Ajarostaghi et al. [13] studied a horizontally oriented finned shell-and-tube heat exchanger containing PCM. They stated that due to the buoyancy effects, the upper part of the heat exchanger melts sooner than the lower portion. Also, they examined the HTF arrangement and showed that the complete melting time was reduced by 69.14 % for the case with a double vertical array of HTF tubes and a double

ACCEPTED MANUSCRIPT

vertical arrangement of fins. To address non-uniform melting rates in horizontal shell-and-tube heat exchangers, innovative designs involving fins at the bottom portion with non-uniform distribution have been proposed by Tang et al. [14]. These designs have shown significant improvements, with melting time decreasing by up to 84% and thermal storage density increasing by 466% in certain cases. Experiments and numerical simulations have demonstrated that a semi-circular design can effectively address mismatched melting rates in shell-and-tube heat exchangers by improving the melting rate as the inner tube approaches the lower surface of the outer shell [15].

In horizontal heat exchangers, natural convection significantly impacts the melting process in the upper section, whereas vertical heat exchangers experience ongoing natural convection throughout the melting process [16]. Researchers have scrutinized the influence of parameters such as the number of fins, length, thickness, and position angle on the melting process of RT35 in a vertical shell and tube heat exchanger, identifying optimal conditions to minimize melting time [17, 18]. Safari et al. [19] delved into the combined effect of fin configuration and tube eccentricity on heat transfer and PCM melting rate within a vertical shell-and-tube heat exchanger, observing that the presence of bifurcations in the fins reduces the convective heat transfer coefficient while increasing the total heat transfer rate. Ebrahimnataj et al. [20] proposed a model featuring T-shaped fins in a vertical triple-tube PCM storage unit in which the PCM is placed in the middle tube. Also, the HTF flows through the inner and outer tubes. They simulated different cases including No-Fin, Uniform-Fin (straight fin) and T-shaped-Fin. Results showed that for the heat exchanger with optimum T-shaped fins, the complete melting time is significantly reduced. Khedher et al. [21] conducted an experimental and numerical study on a vertical triple-tube LHTS system, focusing on enhancing heat transfer by incorporating metal fins and 1% CNT and 2% Al2O3 nanoparticles. Results showed that the use of nano-enhanced PCM with 1% CNT and placement of six external and internal longitudinal fins reduces the discharge and charge time by more than 80%.

Mehta et al. [22] investigated the thermal performance of shell and tube heat exchangers in both vertical and horizontal configurations, concluding that in horizontal heat exchangers, the upper half melts earlier due to natural convection, while in vertical heat exchangers, the melting front becomes conical, with the

ACCEPTED MANUSCRIPT

upper part exhibiting a higher melting rate due to natural convection. Shahsavar et al. [23] found that employing a corrugated inner tube in a vertical double-pipe heat exchanger reduced melting and freezing times compared to a straight tube. Najim et al. [24] studied the effect of different dimensions of circular fins in a vertical triple-tube heat exchanger, discovering that non-uniform fins reduced the time for complete melting by 10.4% compared to uniform fins. Dai et al. [25] explored the melting and freezing processes in a vertical triplex-tube heat exchanger, suggesting that gradually altering the diameters of the inner and middle tubes can increase the rate of phase change. In other words, they suggested that the inner tube should be a cone with its diameter increasing in the direction of the flow, and the middle tube should have the opposite condition. In their study, PCM is located between the inner and outer tubes. The results show that the conical structure significantly increases the charging rate. Zhang et al. [26] focused on the evaluation of thermal storage performance with different helix pitches and fin numbers. The findings indicate that reducing helix pitch and increasing fin number can accelerate the melting process, but these choices should consider performance and processing concerns. Moreover, the orientation of the device, especially when placed horizontally, and the use of oscillating inlet temperature can significantly reduce melting times. Chen et al. [27] investigated the impact of incorporating annular fins with nonuniform distribution on the thermal response of PCM in a vertical triple-tube heat exchanger. The main focus is on determining the best locations and sizes of the fins to achieve the highest storage performance. Results show that optimized fin distribution can lead to significant improvements in melting and solidification times, with potential savings of up to 29% in melting time and 37% in charging rate.

Recovering residual heat is typically utilized in latent energy storage systems, and given the variable and intermittent nature of this heat [28], it is logical to employ a variable inlet temperature to better reflect real-world conditions. A survey of existing literature reveals that most studies have operated under the assumption of a constant inlet temperature, with only a few instances experimenting with variable boundary conditions [26, 29, 30]. Additionally, vertical heat exchangers have not received as much scrutiny as their horizontal counterparts. As a result, there has been little investigation into how changes in heat transfer rates and phase changes occur in vertical heat exchangers with uniform and non-uniform

ACCEPTED MANUSCRIPT

fin arrangements under alternating boundary conditions. From a pragmatic standpoint, an effective fin distribution within the heat exchanger not only enhances the melting rate but also staves off the need for additional fins, which would otherwise inflate initial costs and construction efforts while diminishing latent energy storage capacity. Therefore, the present paper investigates the melting and freezing of PCM in a vertical double-tube heat exchanger with uniform and non-uniform arrangement of fins under constant and intermittent boundary conditions. For this purpose, three different fin arrangements including uniform distribution and two non-uniform distributions corresponding to two geometric progressions 2 and 3 have been investigated. The effect of each arrangement has been investigated separately on the melting and storage rate of latent, sensible and total energies for constant and intermittent boundary conditions.

2- Problem definition and assumptions

Geometry of the problem involves a vertical double-tube heat exchanger with concentric tubes. The dimensions and geometry of this heat exchanger are shown in Fig. 1. RT50 exists as PCM in the annular space between two vertical tubes. Water enters the inner tube as HTF from the bottom with a mass flow rate of 1.60 kg/s and a velocity of 0.043 m/s and exits from the other side at atmospheric pressure.

According to Fig. 1a and due to symmetry of the geometry and the effects of natural convection, the problem can be solved two-dimensionally along the axis-z (Fig. 1b). Also, to compensate for the poor conductivity of the PCM, metal annular fins made of copper are suggested (Fig. 1c). Thermophysical properties of RT50, water, and copper are reported in Table 1. Four fins with thickness t_F=2 (mm) and length l_F=20 (mm) are used at different positions with the distance a on the inner tube surface. In general, the dimensions and size of the double-tube heat exchanger are constant in all cases, and only the location of the fins changes. The simulations have been performed using the following simplifying assumptions:

1- Since the heat exchanger is considered vertical, the effects of natural convection in the angular direction can be ignored. Therefore, the current problem will be solved in two dimensions applying the axial symmetry.

ACCEPTED MANUSCRIPT

2- Thermophysical properties of the PCM are constant and independent of temperature.

3- Natural convection is applied during the PCM melting with the Boussinsque approximation.

4- The effects of viscous losses are not considered in the energy equation.

5- The PCM is homogeneous and isotropic in solid and liquid phases.

6- Volume changes due to the melting of the PCM have been ignored.

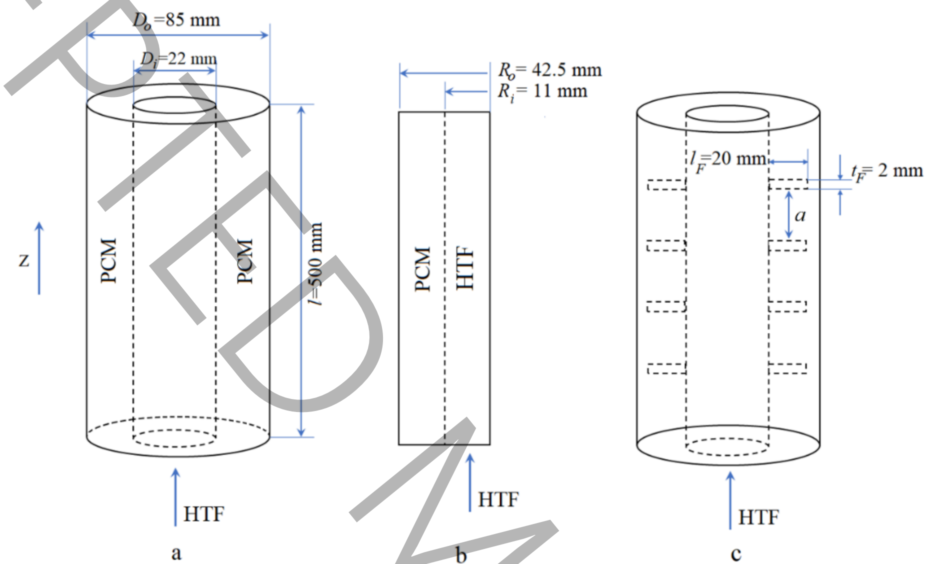

Fig. 1 Schematic of a heat exchanger: a) 3D view of a finless heat exchanger, b) 2D view of a finless heat exchanger, c) 3D view of a heat exchanger with uniform fin distribution.

Table 1. Thermophysical properties of RT50, water, and copper fins [16].

Material	Specific heat capacity, c_p (J/kg.K)	Thermal conductivity, k (W/m.K)	Density, ρ (kg/m^3)	Specific latent heat, L (J/kg)	Melting temperature, T_s, T_l (K)	Volumetric thermal expansion coefficient, β (1/K)
RT50	2000	0.2	880	168000	318-324	0.0006
Water	4182	0.6	998.2	---	---	---
Copper	381	387.6	8978	---	---	---

3- Physical model

In this section, the conservation equations of mass, momentum and energy are given along with initial and boundary conditions. Also, the details of numerical solution and discretization of the equations are mentioned.

ACCEPTED MANUSCRIPT

3-1- Governing equations

According to Fig. 1b and assuming axial symmetry, the problem is formulated in a two-dimensional form using cylindrical coordinates r and z. Based on the assumptions, the continuity equation for the PCM is written as follows [31]:

$$\frac{1}{r}\frac{\partial(ru_r)}{\partial r}+\frac{\partial(u_z)}{\partial z}=0 \tag{1}$$

where, u_r and u_z are the velocity in r and z directions, respectively. The conservation equation of momentum for the PCM in the r direction is given by [32]:

$$\rho\left[\frac{\partial u_r}{\partial t}+u_r\frac{\partial u_r}{\partial r}+u_z\frac{\partial u_r}{\partial z}\right]=\frac{-\partial p}{\partial r}+\mu\frac{\partial^2 u_r}{\partial z^2}+\mu\frac{1}{r}\frac{\partial}{\partial r}\left(r\frac{\partial u_r}{\partial r}\right)-\mu\frac{u_r}{r^2}+Au_r \tag{2}$$

where, ρ, p, μ and A are the density, pressure, dynamic viscosity and porosity function, respectively. The momentum conservation in the z direction for the PCM is also written as:

$$\rho\left[\frac{\partial u_z}{\partial t}+u_r\frac{\partial u_z}{\partial r}+u_z\frac{\partial u_z}{\partial z}\right]=\frac{-\partial p}{\partial z}+\mu\frac{1}{r}\frac{\partial}{\partial r}\left(r\frac{\partial u_z}{\partial r}\right)+\mu\frac{\partial^2 u_z}{\partial z^2}+Au_z+S_b \tag{3}$$

where, the source S_b is related to the buoyancy force, and is given using the Boussinesq approximation:

$$S_b=\rho g\beta\left(T-T_{ref}\right) \tag{4}$$

where, β is the volumetric thermal expansion coefficient of the PCM, g is acceleration due to gravity, T is the temperature of the PCM, and T_{ref} expresses the reference temperature. The porosity function, A is given in the following form [31]:

$$A=\frac{-c(1-\gamma)^2}{\gamma^3+\varepsilon} \tag{5}$$

where $\varepsilon=10^{-3}$ is a small value that prevents the denominator from becoming zero when the liquid fraction, γ becomes zero. The mushy zone parameter c is considered 10^5. The liquid fraction can be obtained by:

ACCEPTED MANUSCRIPT

ACCEPTED MANUSCRIPT

$$\gamma = \begin{cases} 0 & T < T_s \\ \dfrac{T - T_s}{T_l - T_s} & T_s < T < T_l \\ 1 & T > T_l \end{cases} \tag{6}$$

where T_l and T_s indicate the temperature of the beginning and end of the melting, respectively.

The energy conservation equation is the same for both solid and liquid phases in the enthalpy-porosity method. In this method, the porosity value equals one for the liquid phase and zero for the solid phase. The area between solid and liquid is called the mushy zone, and the porosity of this area is between zero and one. The energy conservation equation in terms of total enthalpy and ignoring the viscous losses is as follows:

$$\frac{\partial(\rho H)}{\partial t} + \mathbf{u}.(\nabla H) = k\nabla^2 T \tag{7}$$

where, **u** is the velocity vector and k is the conductivity of the PCM. The total enthalpy H, is expressed as the sum of the sensible h and the latent enthalpies ΔH:

$$H = h + \Delta H \tag{8}$$

where the latent enthalpy is calculated from the product of latent heat of melting, L in the liquid fraction, $\Delta H = \gamma L$. Also, the sensible enthalpy in Eq. (8) can be obtained by:

$$h = h_{ref} + \int_{T_{ref}}^{T} c_p \Delta T \tag{9}$$

where, h_{ref} is the reference enthalpy at the reference temperature and c_p indicates the specific heat of the PCM. By inserting Eqs. (8) and (9) into Eq. (7), the energy equation is obtained as:

$$\frac{\partial(\rho h)}{\partial t} + \frac{\partial(\rho \Delta H)}{\partial t} + \frac{1}{r}\frac{\partial(r\rho u_r h)}{\partial r} + \frac{\partial(\rho u_z h)}{\partial z} = k\left(\frac{1}{r}\frac{\partial}{\partial r}\left(r\frac{\partial T}{\partial r}\right) + \frac{\partial^2 T}{\partial z^2}\right) \tag{10}$$

The contribution of latent E_l and sensible E_s energies of the PCM can be obtained separately by the following equations:

$$E_l = \int_V (\rho \gamma L) dv \tag{11}$$

$$E_S = \int_V \left(\rho c_p (T - T_{in})\right) dv \tag{12}$$

where T_{in} is the initial temperature of the system. The total energy E of the PCM is also obtained from the sum of the sensible and latent energies:

$$E = E_s + E_l \tag{13}$$

3-2- Boundary and initial conditions

The HTF enters the heat exchanger in two cases of constant and intermittent conditions. However, due to the high flow rate and high heat capacity of the HTF (water), the temperature changes of the HTF along the heat exchanger are expected to be negligible. This helps to use a prescribed temperature in the inner wall of the heat exchanger, $r=R_i$ [16]. The accuracy of this assumption will be proved in section 5-1. For the case of constant temperature and at $r=R_i$, one has:

$$T(R_i, z, t) = T_b \tag{14}$$

where T_b=343 K is the HTF temperature. For the intermittent condition and at $r=R_i$, the following sine equation may be assumed:

$$T(R_i, z, t) = T_l + \zeta \sin(\omega t) \tag{15}$$

where, ζ is the amplitude, and ω is the HTF temperature frequency. The outer shell wall of the heat exchanger, $r=R_o$ and the upper and lower walls of the system are considered adiabatic.

ACCEPTED MANUSCRIPT

$$\frac{dT\,(R_o, z, t)}{dr} = 0 \tag{16}$$

$$\frac{dT\,(r, 0, t)}{dr} = 0 \qquad (R_i \le r \le R_0) \tag{17}$$

$$\frac{dT\,(r, l, t)}{dr} = 0 \qquad (R_i \le r \le R_0) \tag{18}$$

Also, the following expression is used to apply the initial condition:

$$T\,(r, z, 0) = T_{in} \tag{19}$$

where T_{in} =293 K. Considering the initial temperature and comparing it with the freezing temperature, the initial state of PCM will be solid.

The Fluent application of the ANSYS 16 software is used for numerical simulation and solving the governing equations. The pressure-based discretized equations are used to solve the governing equations due to the incompressibility of the problem. Also, the coupled algorithm is used to solve the velocity and pressure equations. The PRESTO method is selected to discretize the pressure equations, and the second-order upwind method is set to discretize the momentum and energy equations. The enthalpy-porosity technique solves the melting and freezing problems. In this method, the desired domain is assumed to be a porous medium, where the porosity value is 0 in the solid phase and 1 in the liquid phase. The solid-liquid interface, has a porosity between 0 and 1, and the position of the solid-liquid interface is explicitly determined at every moment [33].

4- Validation, mesh and time step independencies

To validate the numerical simulation of the PCM melting inside a heat exchanger, the results of Mat et al. [34] is selected. In this work, a triplex-tube heat exchanger with fins 42 mm long is designed in such a way that four fins are connected to the wall of the inner tube and four fins are connected to the outer tube. Their experimental investigation consists of a horizontal triplex-tube heat exchanger, where RT82 is used

ACCEPTED MANUSCRIPT

as a PCM, and water flows as the HTF in the inner and outer tubes. In addition to reporting the liquid fraction, the average temperature of 15 temperature sensors that are radially distributed in four different angles help to perform the validation. The validation results are obtained after checking the independence of the results from the mesh and the time step sizes. Therefore, the final grid size and time-step are 24560 and 0.5 (s), respectively. Fig. 2 compares the average temperature of the sensors T_m between the current work and those of Mat et al. [34]. Based on this figure, the smallest relative error between the numerical and experimental temperature evaluations (excluding the initial time) is 0.97% at t=35 (s), while the largest relative error is observed at t=5 (s), amounting to 7.43%, and the mean relative error is 3.79%. Furthermore, Fig. 3 illustrates the variations in liquid fraction over time. As per this figure, the lowest relative error between the current work and the results of [34] in the evaluation of liquid fraction (excluding the initial time) is 0.63% at t=41.7 (s), with the highest relative error occurring at t=21.4 (s) and reaching 16.07%. The mean relative error for this case is 8.85%. Consequently, there is a satisfactory agreement between the outcomes of this study and the available results of [34].

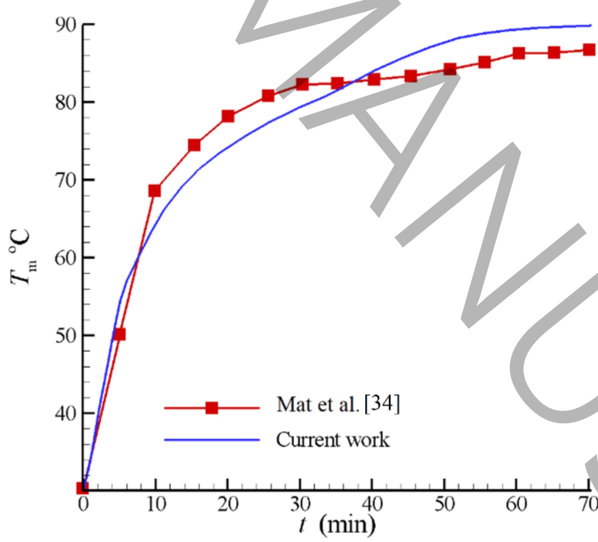

Fig. 2 Changes in the average temperature of the sensors between the current work and the experimental results of Mat et al. [34].

ACCEPTED MANUSCRIPT

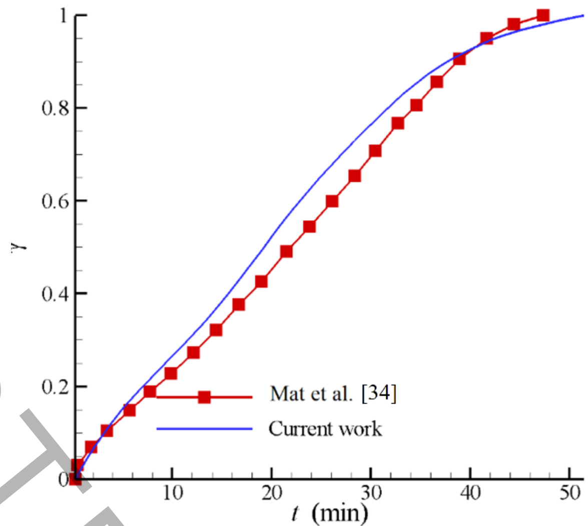

Fig. 3 Changes in the liquid fraction between the current work and the numerical results of Mat et al. [34].

Also, it's important to verify that the numerical results are not dependent on the mesh size and time step. Fig. 4 depicts the variation of liquid fraction with time in a finless heat exchanger for different mesh sizes at Δt=0.1 (s). From this figure, it is observed that at t=14000 (s) and Δt=0.1 (s), the maximum difference in liquid fraction between the grid sizes of 3600 and 8000 is 1.4%. Consequently, a grid size of 3600 is chosen for all cases. To confirm result independence from the time step, three time-steps (Δt=0.03 (s), Δt=0.1 (s), and Δt=0.3 (s)) are selected, and simulations are conducted using the final grid size of 3600. Fig. 5 demonstrates that the difference in liquid fraction between Δt=0.1 and Δt=0.03 (s) at t=14000 (s) is less than 0.4%. Thus, to decrease computational costs, a time step of 0.1 (s) is utilized for all simulations.

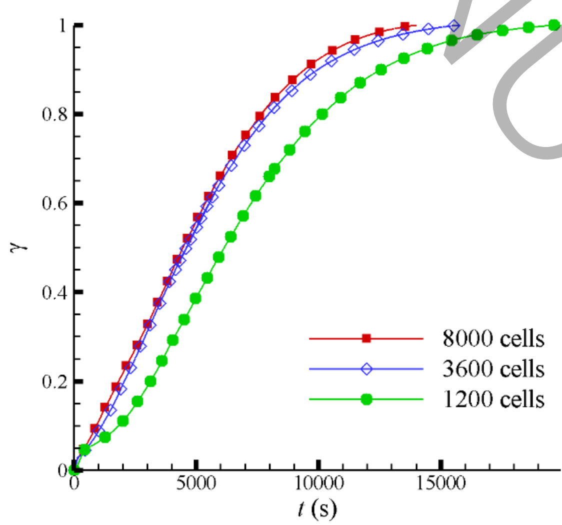

Fig. 4 Variation of the liquid fraction over time in a double-tube finless heat exchanger for different grid sizes, Δt=0.1 (s).

ACCEPTED MANUSCRIPT

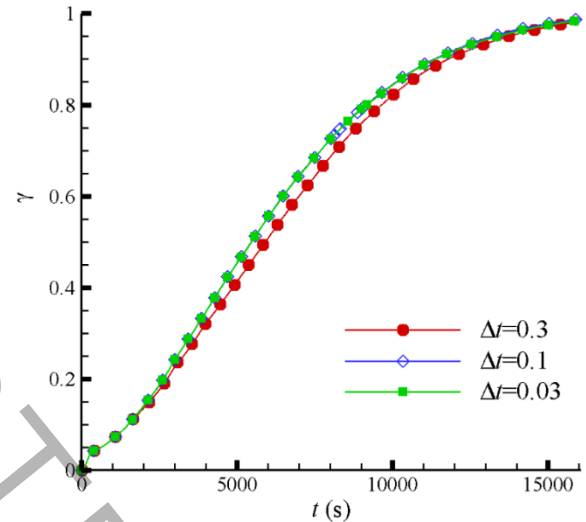

Fig. 5 Variation of liquid fraction over time in a double-tube finless heat exchanger for different time steps when the grid size is 3600 cells.

5- Results and discussion

In the initial part of this section, the problem's conditions are assessed to enable the application of specified temperature boundary conditions. The subsequent subsection delves into the investigation of the melting process within a vertical double-tube heat exchanger under constant boundary conditions. This subsection is further divided into two parts: examination of the heat exchanger with a uniform distribution of fins (including an inquiry into a finless heat exchanger) and an analysis of the heat exchanger with non-uniform fin distribution. Following this, the authors scrutinize the melting process under intermittent temperature conditions of the HTF and conclude by examining the changes in sensible, latent, and total energies.

5-1- Applying the prescribed inlet temperature

When the high mass flow rate of the HTF is utilized during the melting process, its temperature remains stable. This is demonstrated by examining the heat transfer rate Q over time for a finless heat exchanger, as depicted in Fig. 6. Heat transfer rate is calculated by deriving the total energy of the PCM, E, with respect to time: $Q=\mathrm{d}E/\mathrm{d}t$. In Fig. 6, it is observed that despite the substantial energy stored in the PCM, the average heat transfer rate, Q_m, ranges around 137.7 W from 158 to 6300 seconds. Considering the heat

ACCEPTED MANUSCRIPT

capacity and mass flow rate of water (1.6 kg/s), the temperature difference between the HTF's inlet and outlet is less than 0.02 °C. Initially, there might be a slight rise in water temperature by over 0.02 °C before 158 seconds. However, given that the simulation duration significantly exceeds this period by more than 30 times, and the liquid fraction is under 1.5% initially (see Fig. 13), it is reasonable to neglect temperature variations in the water flow within the tube.

Notably, based on the flow rate through the inner tube, water's thermophysical properties, and tube geometry, the Reynolds number of the flow reaches approximately 93000. Consequently, the convective heat transfer coefficient surpasses 12800 ($W/m^2.K$) following the Dittus–Boelter correlation. With such a high convection coefficient, a prescribed temperature boundary condition can be applied to the tube, assuming the wall temperature is equal to the inlet temperature due to the small difference between the inlet and outlet temperatures of the tube. In instances where thin fins are present on the outer surface of the inner tube, it is still plausible to assume a prescribed temperature distribution across the tube and fin wall. Employing a fin of 2 mm thickness in the current study facilitates maintaining this assumption.

5-2- Constant temperature of the HTF

5-2-1- Heat exchanger with uniform distribution of fins

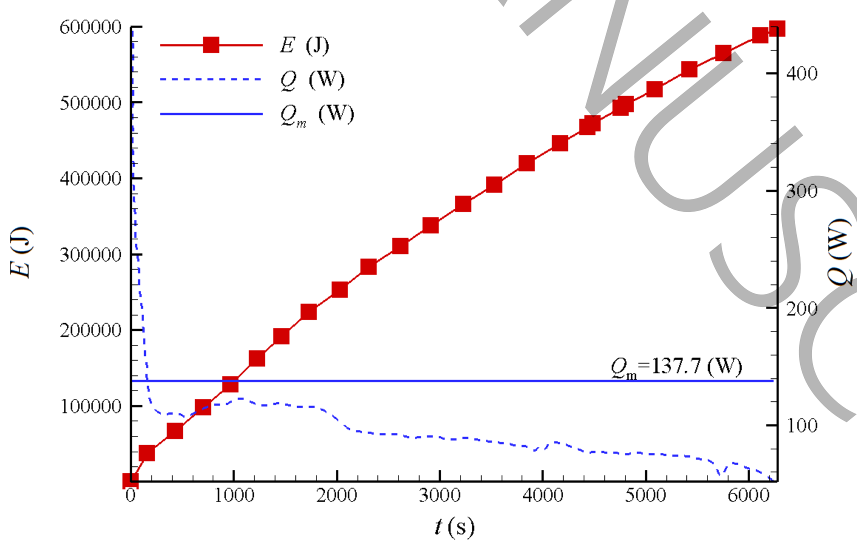

Fig. 6 Variations of the total energy of the PCM and the heat transfer rate over time for a finless heat exchanger.

ACCEPTED MANUSCRIPT

Fig. 7 shows the liquid fraction contours with the streamlines for a finless heat exchanger at t=30, t=60, t=120, and t=180 (min), respectively. It is seen that the dominant mechanism of heat transfer in the early times is conduction, and only in the small part above the heat exchanger, the effects of natural convection appear. Fig. 8 shows the temperature contour with the streamlines for a finless heat exchanger. This figure states that natural convection in a finless heat exchanger creates a temperature difference between the upper and lower parts of the heat exchanger.

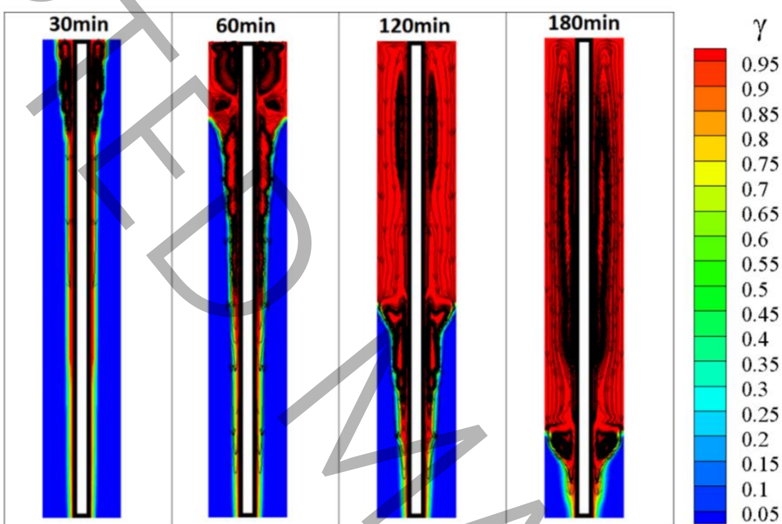

Fig. 7 Liquid fraction contours with streamlines at t=30 (min), t=60 (min), t=120 (min), and t=180 (min) for a finless heat exchanger.

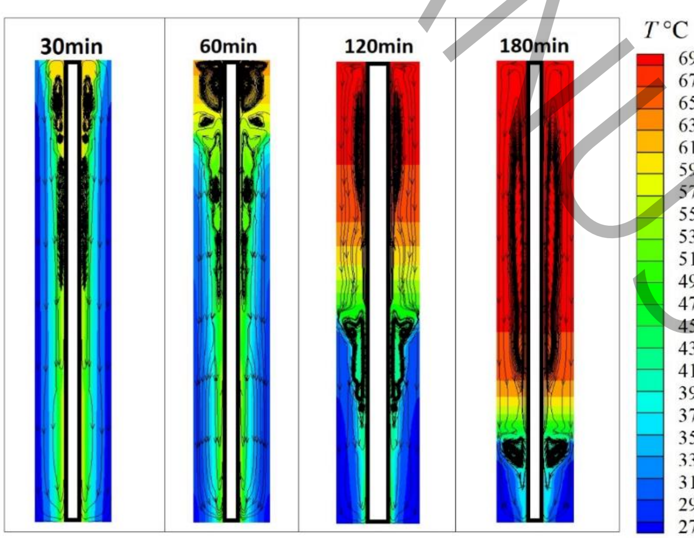

Fig. 8 Temperature contours with streamlines at t=30 (min), t=60 (min), t=120 (min), and t=180 (min) for a finless heat exchanger.

ACCEPTED MANUSCRIPT

The noticeable point is the positive effect of natural convection in increasing the melting rate in the upper part of the heat exchanger. This point suggests using fins at the bottom of the heat exchanger to make the heat transfer rate more uniform throughout the heat exchanger. Fig. 9 displays the liquid fraction for a finned heat exchanger where the fins are uniformly spaced at 100 (mm) from each other. The comparison of Fig. 7 and Fig. 9 shows that the presence of fins increased heat penetration to the inner layers of PCM and reduced the melting time. Also, it is seen that the presence of fins with equal distances significantly reduces the melting time of the PCM and creates uniformity in the melting process between the upper and lower parts of the heat exchanger. According to Fig. 10, the presence of fins with the same distance causes the creation of similar vortices between the fins. These similar vortices, together with the uniform distribution of the fins, have caused simultaneous melting in the heat exchanger, except for the lower part where the effects of natural convection are weak.

5-2-2- Heat exchanger with non-uniform distribution of fins

As natural convection has a significant impact in the upper region of the heat exchanger, denser placement of fins in this area not only lacks benefits, but can also compromise natural convection. Conversely, due to the diminished heat transfer rate in the lower portion of the heat exchanger, the installation of fins with a denser distribution in this section can enhance the rate of heat transfer and melting without concern for impeding natural convection. Therefore, employing fins in a geometric progression, where the distance from the bottom to the top is set with a common ratio of *q* and the scale factor of *a*, would be advantageous. Consequently, the distance of the first fin from the bottom of the heat exchanger is *a*, and the distances of the fins from *n*=2 to *n*=4 are calculated using the following equation:

$$a_n = aq^{n-1} \tag{20}$$

In this study, two different common ratios, *q*=2 and *q*=3, are utilized. With *q*=2, the distances of the fins from the bottom of the tube are 10, 20, 40, and 80 (mm), while with *q*=3, these distances are 10, 30, 90, and 270 (mm). As illustrated in Fig. 11 and Fig. 12, arranging the fins in a geometric progression leads to a more even melting across the heat exchanger over time, ensuring that the PCM in the lower part of the

ACCEPTED MANUSCRIPT

heat exchanger melts completely simultaneously with the other parts. It is observed that for the heat exchangers with uniform fin distribution and geometric progressions q=2 and q=3, the total melting time is 9630, 6280, and 5100 (s), respectively. This represents a reduction in melting time of 53%, 69%, and 75% compared to the finless heat exchanger, respectively.

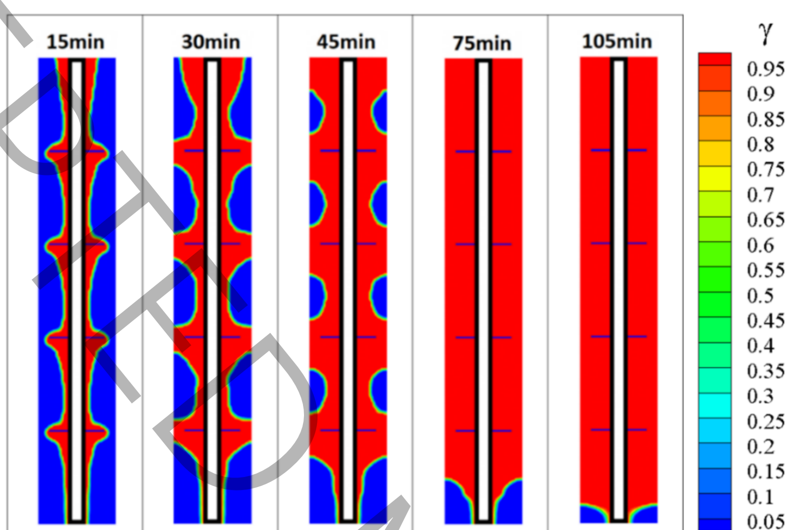

Fig. 9 Liquid fraction contours at t=15 (min), t=30 (min), t=45 (min), t= 75 (min), and t=105 (min) for a heat exchanger with uniform distribution of fins.

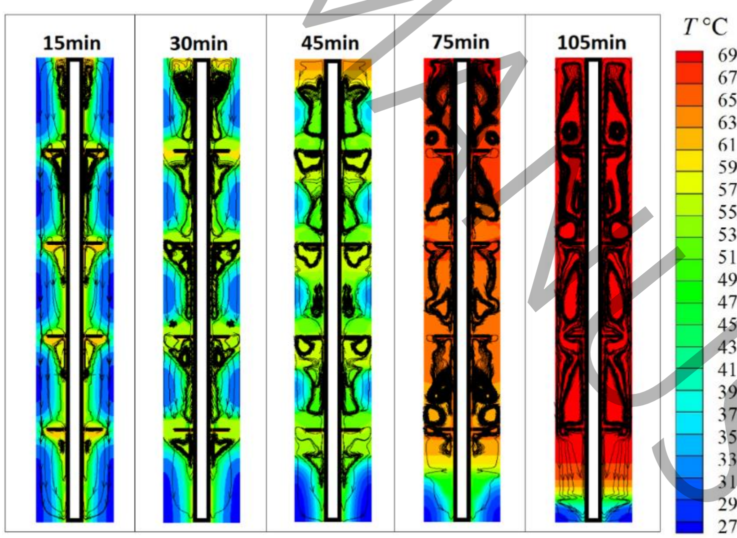

Fig. 10 Temperature contours at t=15 (min), t=30 (min), t=45 (min), t= 75 (min), and t=105 (min) for a heat exchanger with uniform distribution of fins

ACCEPTED MANUSCRIPT

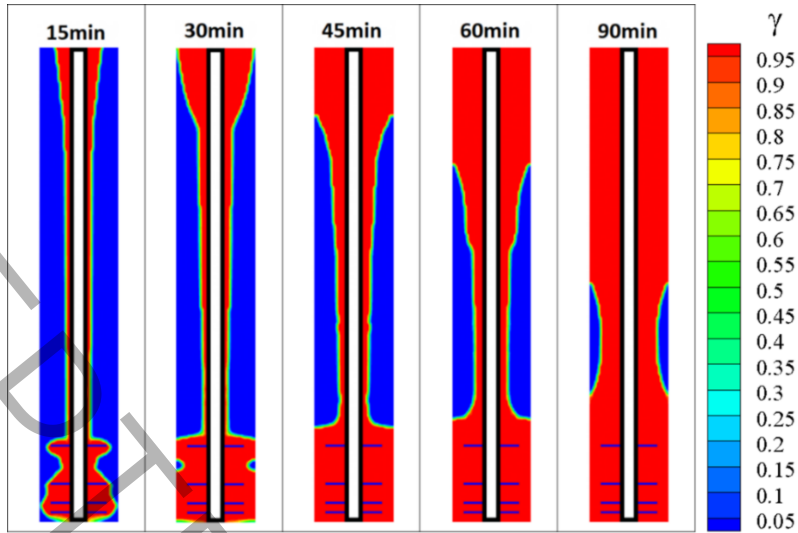

Fig. 11 Liquid fraction contours for non-uniform distribution of fins with q=2.

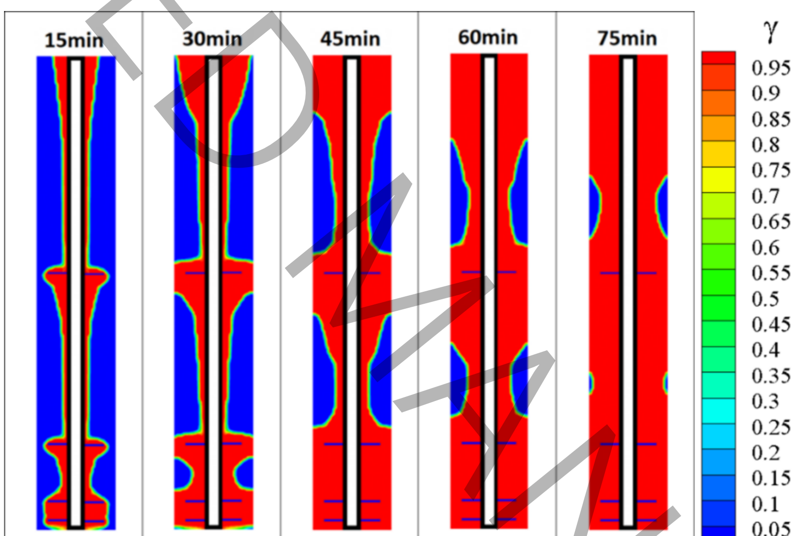

Fig. 12 Liquid fraction contours for non-uniform distribution of fins with q=3.

Fig. 13 depicts the variations in liquid fraction over time for different arrangements of fins. As anticipated, the inclusion of fins accelerates the melting rate. Additionally, a noticeable shift in the slope of the liquid fraction is observed for the uniform fin distribution, occurring when approximately 10% of the PCM remains solid in the heat exchanger. Illustrated in Fig. 9, this solid portion persists in the lower section of the heat exchanger, distant from the fins and the effects of natural convection. The melting conditions in this segment resemble those of a finless heat exchanger, hence the rate of liquid fraction change beyond this point aligns with the pattern of a heat exchanger without fins.

ACCEPTED MANUSCRIPT

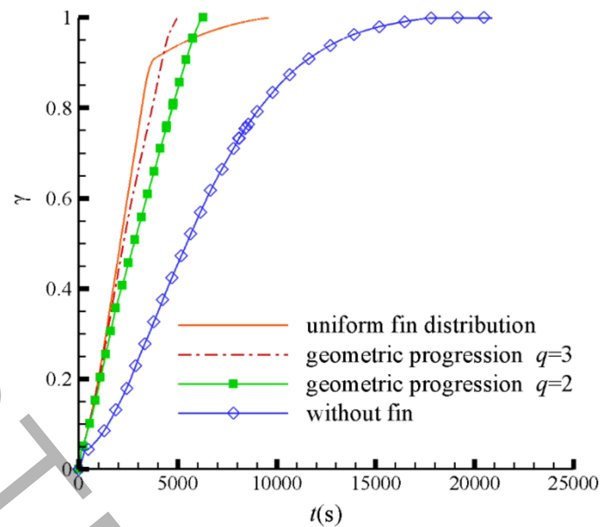

Fig. 13 Changes of PCM liquid fraction with time for different fin arrangements.

Notably, the complete melting time is 20700 (s) for a finless heat exchanger and 9630 (s) for a heat exchanger with uniformly distributed fins, indicating a 53% reduction in melting time due to the presence of four equally spaced fins. Furthermore, for heat exchangers with uniform fin distribution and geometric progressions of q=2 and q=3, the total melting times are 9630, 6280, and 5100 (s), signifying reductions of 53%, 69%, and 75% compared to the finless heat exchanger, respectively.

It should be noted that during the melting process, the phase of the PCM begins as solid and transitions to a liquid phase as heat is transferred over time. The presence of fins in the heat exchanger enhances heat transfer, leading to increased liquid fraction and reinforcing the rate of heat transfer, as shown in Fig. 13. A comparison of Fig. 11 and Fig. 12 reveals that in case q=2, with more space in the upper part of the heat exchanger for reinforcement of the velocity field, there is a greater solid phase at t=90 (min) compared to case q=3, where the fins may have impeded velocity growth. Therefore, there is no possibility of weakening the melting rate due to weakening of the velocity field and natural convection due to the presence of fins or the formation of a solid phase inside the heat exchanger.

As previously noted, with uniform fin distribution, the rate of PCM melting experiences a significant decline after t=3750 (s), thereafter aligning closely with the finless condition. This indicates that the fins lose their effectiveness beyond 3750 (s). Conversely, in the case of fins with geometric progression, the liquid fraction curve maintains a nearly constant slope, devoid of sudden changes. This phenomenon

ACCEPTED MANUSCRIPT

suggests that the PCM in the lower section of the heat exchanger melts simultaneously with the rest. Additionally, it is evident that the shortest duration for complete melting occurs when q=3.

5-3- Intermittent temperature of the HTF

In section 3-2- a sinusoidal boundary condition is proposed to account for intermittent behavior of the HTF. The fluctuation range in Eq. (15) is assumed to be equal to the difference between the temperature of the HTF under constant temperature conditions and the melting temperature of the PCM (ζ=343-324=19 K). Also, the frequency of HTF temperature can be given by $\omega=2\pi/P$. The period P=5100 (s) is chosen according to the minimum time required for the PCM melting for a common ratio q=3 with constant boundary conditions. The temperature at the beginning of the melting is 324 K, and according to Eq. (15), the temperature of the HTF fluctuates between 305 and 343 K. This issue provides the necessary conditions for simultaneous melting and freezing in a period. In all the calculations of this part, the duration of the simulation is twice the period P.

Figs. 14-17 show the contours of liquid fraction in two cycles (two periods of melting and two periods of freezing), for the finless heat exchanger, heat exchangers with uniform fin distribution and fin distributions with q=2 and q=3, respectively. According to Fig. 14, the PCM experiences both melting and freezing processes in each cycle (less than 85 minutes), so the liquid phase around the inner tube at t=30 (min) freezes again at t=60 (min).

Because in the constant inlet temperature, the temperature is 343 K, but in fluctuating boundary conditions, the boundary temperature changes between 305 K and 343 K, so in fluctuating conditions, the liquid fraction will be lower than in constant melting conditions. This can be seen by comparing Fig. 7 and Fig. 14. This point is important from a practical point of view due to the existence of fluctuations in real conditions. Increasing the complete melting time in fluctuating conditions can eliminate the need to choose a large heat exchanger.

ACCEPTED MANUSCRIPT

ACCEPTED MANUSCRIPT

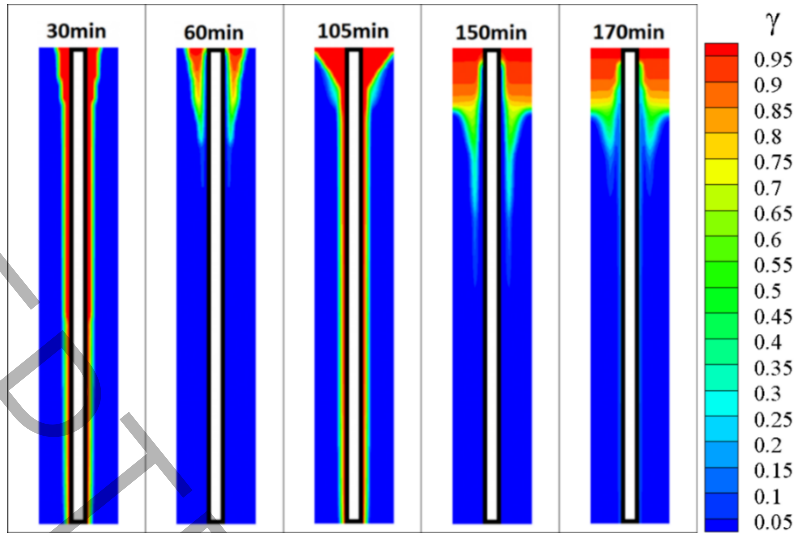

Fig. 14 Liquid fraction contours at *t*=30 (min), *t*=60 (min), *t*=105 (min), *t*=150 (min) and *t*=170 (min) for a finless heat exchanger in the intermittent boundary condition.

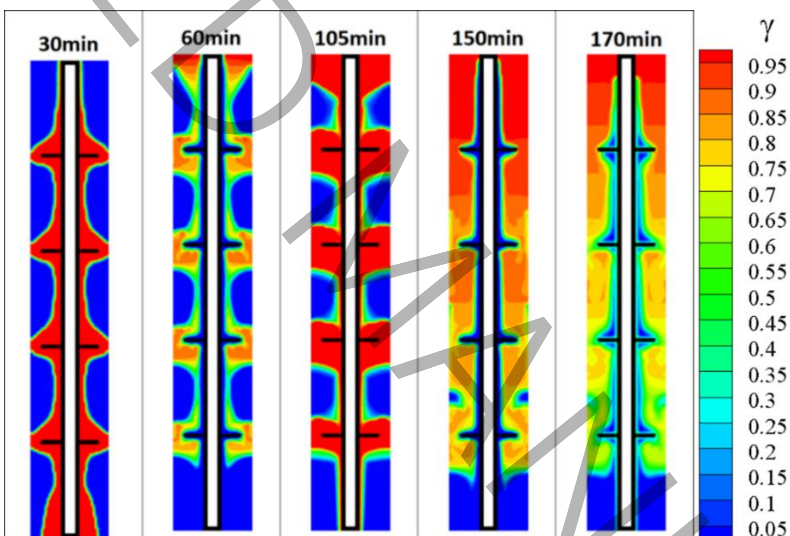

Fig. 15 Liquid fraction contours at *t*=30 (min), *t*=60 (min), *t*=105 (min), *t*=150 (min) and *t*=170 (min) for a heat exchanger with uniform fin distributions in the intermittent boundary condition.

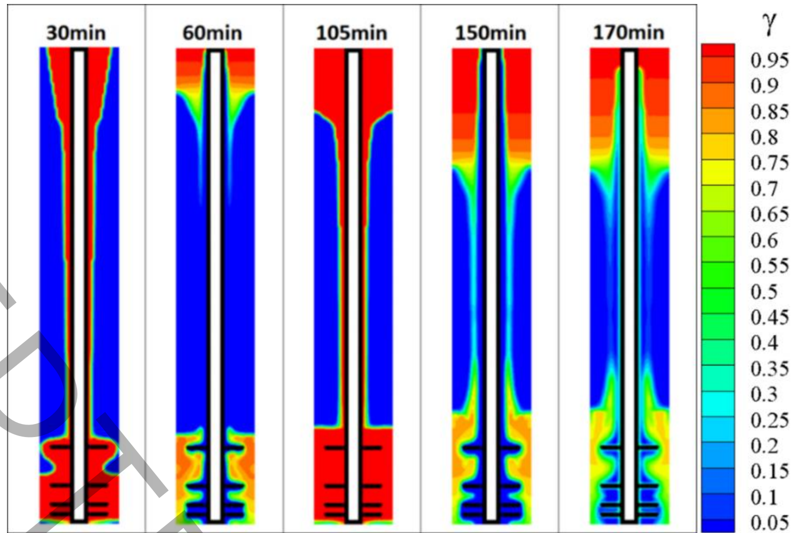

Fig. 16 Liquid fraction contours at t=30 (min), t=60 (min), t=105 (min), t=150 (min) and t=170 (min) for a heat exchanger with progressive distribution q=2 in the intermittent boundary condition.

Another observation apparent in Figs. 14-17 is the substantial volume of the mushy zone at times t=60 and t=150 (min) (minimum temperature of the boundary) in contrast to t=30 (min) and t=105 (min) (maximum temperature of the boundary). To explain this phenomenon, one must consider the contrast between melting and freezing conditions. During melting, heat transfer solely occurs from the inner wall of the tube (HTF side), whereas during freezing, cooling occurs from both the HTF and the solid phase, resulting in a larger mushy zone. The presence of a mushy zone diminishes the velocity field in the liquid phase during freezing compared to the melting process.

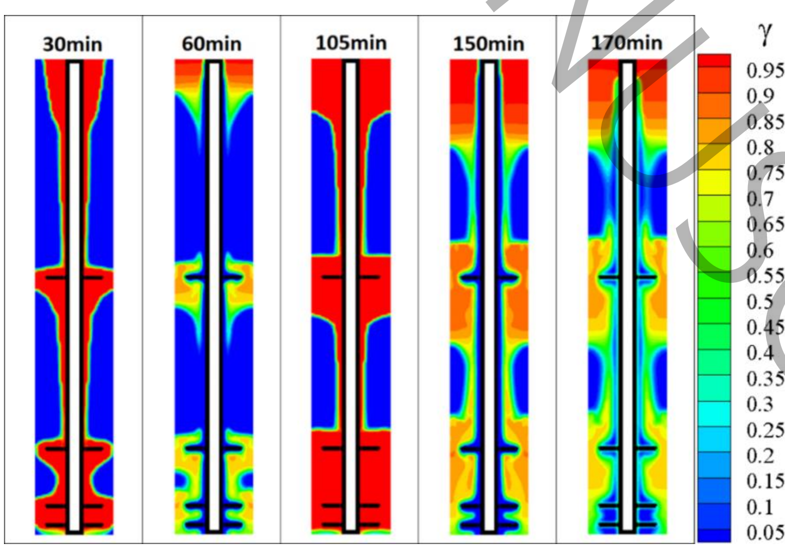

Fig. 17 Liquid fraction contours at t=30 (min), t=60 (min), t=105 (min), t=150 (min) and t=170 (min) for a heat exchanger with progressive distribution q=3 in the intermittent boundary condition.

ACCEPTED MANUSCRIPT

The reduction of the velocity values in the freezing process compared to the melting process for the condition of fins with common ratio q=3 is shown in Fig. 18. Comparison of velocity vectors drawn with 2x magnification shows that the effects of natural convection in the freezing process are negligible.

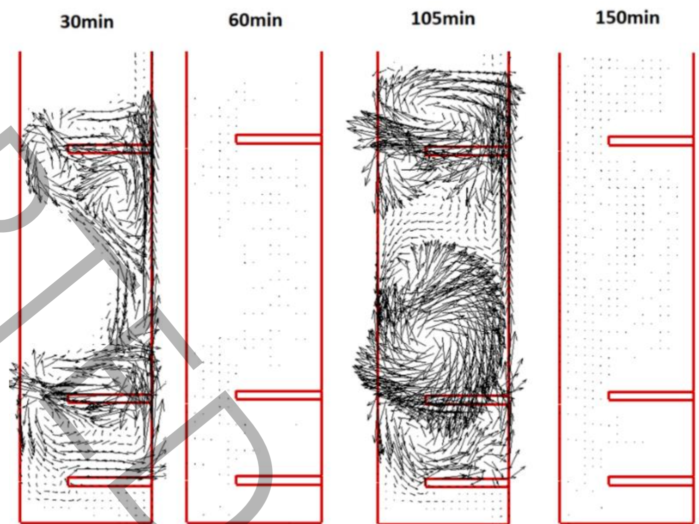

Fig. 18 Velocity vectors at different times for a finned heat exchanger with common ratio of three.

In Fig. 18, two periods of melting and two periods of freezing are shown according to the temperature of the wall. According to this figure, it can be seen that at the end of the melting periods, the liquid fraction immediately decreases and at the end of the freezing periods, the liquid fraction immediately increases. This shows that the creation of liquid phase and solid phase is more influenced by the wall temperature and the sensible energy storage in the liquid phase does not cause the continuation of the melting process in the freezing period, or on the contrary, subcooling the solid phase does not cause the freezing process to continue in the melting period. The large difference between temperature of the solid-liquid interface and the boundary temperature in the melting process (the largest value in the melting process is 343-318=25 K) compared to the freezing process (the largest value in the freezing process is 318-305=13 K) causes a gradual increase in the liquid fraction with time, which is shown in Fig. 19.

Demonstrating the changes in liquid fraction under similar conditions without natural convection is beneficial. Fig. 20 illustrates these changes.

ACCEPTED MANUSCRIPT

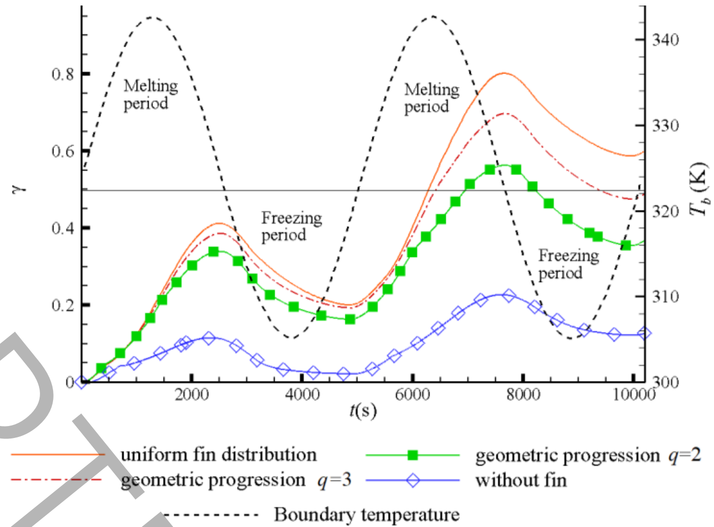

Fig. 19 Variations of liquid fraction with time for different fin arrangements under intermittent boundary conditions.

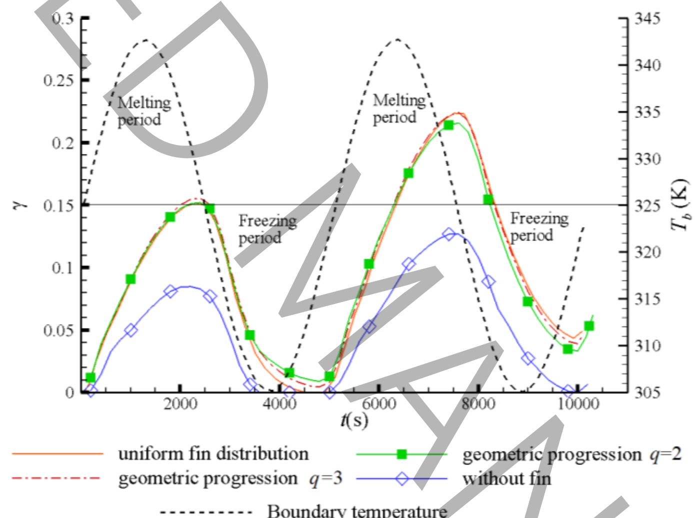

Fig. 20 Variations of liquid fraction with pure conduction for different fin distributions.

A comparison of Fig. 19 and Fig. 20 reveals that the increase in liquid fraction during the melting period is greater under natural convection conditions than under pure conduction assumption. However, the reduction rate of liquid fraction during the freezing period is almost identical for both conditions. Specifically, the increase of liquid fraction during the first melting period is approximately 40% under natural convection, compared to around 15% under pure conduction. Similarly, the reduction in liquid fraction at the end of the first freezing period is approximately 18% with natural convection, only slightly different from the 15% reduction under pure conduction. Thus, it appears that the natural convection affects the melting rate more than the freezing rate. Additionally, during freezing, as the solid phase

ACCEPTED MANUSCRIPT

increases over time, the space for velocity growth in the liquid phase decreases. Conversely, during melting, the space for velocity growth in the liquid phase increases over time. Consequently, in the melting process, the effects of natural convection increase with time.

Finally, the liquid fraction is highest for a heat exchanger with uniform fin distribution, which differs from the results obtained under constant temperature boundary condition, where a heat exchanger with geometric fin distribution of q=3 had the highest liquid fraction.

5-4- Sensible, latent and total energies

Here, the contribution of sensible, latent and total energies for a heat exchanger with different fin arrangements for intermittent boundary condition is investigated. Fig. 21 shows the changes of all three energies stored in a finless heat exchanger with time. It is seen that the contribution of the sensible energy is greater than the latent energy and significant fluctuating behavior is not observed. The lower share of latent energy corresponds to the liquid fraction diagrams drawn in the previous section (Fig. 7). Because the absence of fins has reduced the melting rate and increased the thermal resistance in the heat exchanger. Fluctuation in the latent energy also occurred due to changes in boundary temperature and fluctuation of the liquid fraction.

Fig. 22 shows the changes of energy stored in the PCM for the heat exchanger with uniform fin distribution. The significant difference between Fig. 21 and Fig. 22 is the contribution of latent energy, so that by placing the fin inside the heat exchanger, the contribution of latent energy has increased compared to the sensible one. For example, at t=8000 (s), the latent energy in the finless heat exchanger is 82898 (J) and in the heat exchanger with uniform distribution is 300319 (J). This shows the positive effect of the fin inside the heat exchanger to increase the ability to store the latent energy. The diagram of energy changes for the other two heat exchangers is similar to the last one, but the corresponding figures are omitted for the brevity.

ACCEPTED MANUSCRIPT

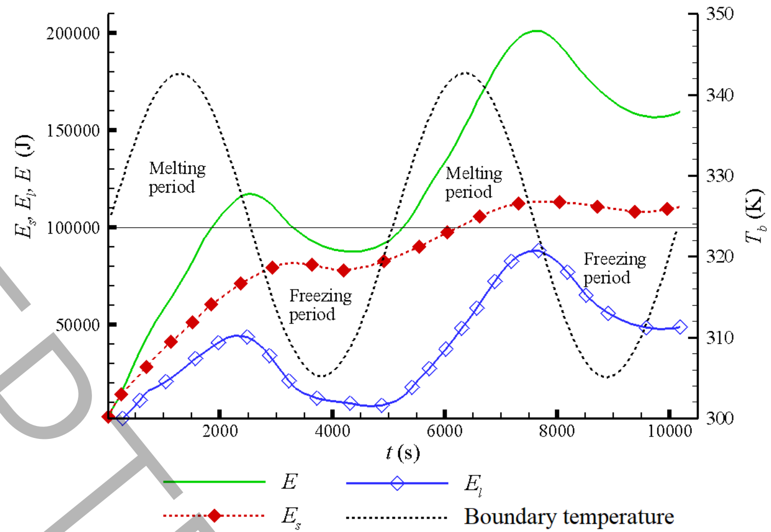

Fig. 21 Total, sensible and latent energy changes in a finless heat exchanger.

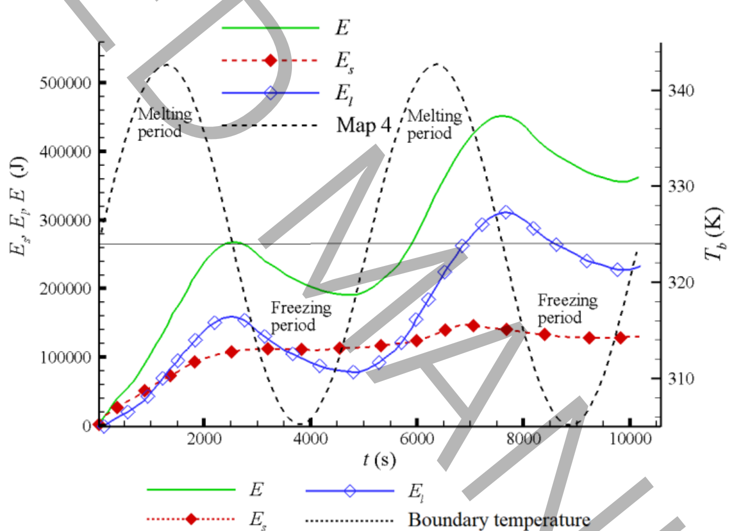

Fig. 22 Total, sensible and latent energy changes in a heat exchanger with uniform fin distribution.

6- Conclusion

The study investigated the melting rate of PCM and its energy storage characteristics in a vertical double-tube heat exchanger, with a specific focus on the fin arrangement under constant and intermittent boundary conditions. The examination involved a vertical finless heat exchanger as well as heat exchangers with uniform and non-uniform fin distributions. For the non-uniform fin distribution,

ACCEPTED MANUSCRIPT

geometric progressions 2 and 3 were utilized, resulting in a higher density of fins in the lower part of the heat exchanger. The principal findings are outlined as follows.

- Under constant temperature boundary conditions, the complete melting time for uniform fin distribution and fin distribution with geometric progressions q=2 and q=3 is reduced by 53%, 69%, and 75% compared to the finless heat exchanger.
- For uniform fin distribution, a noticeable change in the slope of the liquid fraction diagram occurs when approximately 10% of the PCM is solid in the heat exchanger, resembling the melting condition of the remaining part in the finless heat exchanger. Conversely, with fin distribution showcasing geometric progression, the liquid fraction increases uniformly without a sudden drop in the melting slope. In other words, in contrast to uniform fin distribution, the PCM melts at the bottom of the heat exchanger simultaneously with the other parts when the heat exchanger features fin distribution of geometric progression.
- In intermittent boundary conditions, the uniform fin distribution exhibits the highest melting rate. In this scenario, unlike the constant temperature boundary condition, the arrangement of fins in geometric progression does not elevate the liquid fraction. During the melting phase, heat is transferred solely from the HTF side, whereas during the freezing phase, cooling occurs from both the HTF and the solid phase, resulting in a larger mushy zone in comparison with the melting process. This weakens the velocity field in the liquid phase during freezing and diminishes the effects of natural convection in the freezing process compared to the melting process.
- Introducing fins inside the heat exchanger enhances the contribution of latent energy compared to sensible energy due to the increased melting rate in the heat exchanger.

Nomenclature

a_n	Fins distance from the bottom of the heat exchanger, m
A	Porosity function
c_p	Specific heat at constant pressure, J.kg^{-1}.K^{-1}
D_i	Inner tube diameter, m

ACCEPTED MANUSCRIPT

D_o	Outer tube diameter, m
E	Total energy, J
E_l	Latent energy, J
E_s	Sensible energy, J
$\mathbf{g}$	Gravitational acceleration, m.s^{-2}
h	Sensible enthalpy, J.kg^{-1}
H	Total enthalpy, J.kg^{-1}
ΔH	Latent enthalpy, J.kg^{-1}
k	Thermal conductivity, W.m^{-1}.K^{-1}
l	Length of the heat exchanger, m
L_F	Length of the fin, m
L	Latent heat of melting, J.kg^{-1}
p	Pressure, Pa
q	Common ratio
r	Radial coordinates, m
R_i	Inner tube radius, m
R_o	Outer tube radius, m
S_b	Source term, N.m^{-3}
t_F	Thickness of the fin, m
t	Time, s
T	Temperature, K
u_r	Radial velocity, m.s^{-1}
u_z	Axial velocity, m.s^{-1}
$\mathbf{u}$	Velocity vector, m.s^{-1}
z	Axial coordinates, m

Greek symbols

β	Thermal expansion coefficient, K^{-1}
γ	Liquid fraction
ζ	Amplitude of the HTF temperature ,K
μ	Dynamic viscosity, kg.m^{-1}.s^{-1}
ρ	Density, kg.m^{-3}
ω	Frequency of the HTF temperature, s^{-1}

Subscripts

b	Boundary

ACCEPTED MANUSCRIPT

ACCEPTED MANUSCRIPT

in	Initial
l	Liquidus
ref	Reference
s	Solidus

Abbreviations

HTF	Heat transfer fluid
PCM	Phase change material

References

[1] W. Aftab, A. Usman, J. Shi, K. Yuan, M. Qin, R. Zou, Phase change material-integrated latent heat storage systems for sustainable energy solutions, Energy & Environmental Science, 14(8) (2021) 4268-4291.

[2] A.T. Muzhanje, M. Hassan, H. Hassan, Phase change material based thermal energy storage applications for air conditioning, Applied Thermal Engineering, (2022) 118832.

[3] R.A. Lawag, H.M. Ali, Phase change materials for thermal management and energy storage: A review, Journal of Energy Storage, 55 (2022) 105602.

[4] Z. Qu, W. Li, W. Tao, Numerical model of the passive thermal management system for high-power lithium ion battery by using porous metal foam saturated with phase change material, International Journal of hydrogen energy, 39(8) (2014) 3904-3913.

[5] Z.A. Qureshi, H.M. Ali, S. Khushnood, Recent advances on thermal conductivity enhancement of phase change materials for energy storage system: a review, International Journal of Heat and Mass Transfer, 127 (2018) 838-856.

[6] S. Wu, T. Yan, Z. Kuai, W. Pan, Thermal conductivity enhancement on phase change materials for thermal energy storage: A review, Energy Storage Materials, 25 (2020) 251-295.

[7] B.K. Choure, T. Alam, R. Kumar, A review on heat transfer enhancement techniques for PCM based thermal energy storage system, Journal of Energy Storage, 72 (2023) 108161.

[8] س.ا. فنایی, م. رضایی, The Investigation of Appendages Vortex Effect on the Main working Parameter of the Tube-finned Heat Exchanger, مهندسی مکانیک دانشگاه تبریز, ۴۷(۳) (۲۰17) 333-338.

[9] Y. Pahamli, M. Hosseini, A. Ranjbar, R. Bahrampoury, Inner pipe downward movement effect on melting of PCM in a double pipe heat exchanger, Applied Mathematics and Computation, 316 (2018) 30-42.

[10] M.S. Mahdi, H.B. Mahood, A.F. Hasan, A.A. Khadom, A.N. Campbell, Numerical study on the effect of the location of the phase change material in a concentric double pipe latent heat thermal energy storage unit, Thermal Science and Engineering Progress, 11 (2019) 40-49.

[11] H. Xu, N. Wang, C. Zhang, Z. Qu, M. Cao, Optimization on the melting performance of triplex-layer PCMs in a horizontal finned shell and tube thermal energy storage unit, Applied Thermal Engineering, 176 (2020) 115409.

[12] J.R. Patel, M.K. Rathod, R.M. Elavarasan, Z. Said, Influence of longitudinal fin arrangement on the melting and solidification inside the triplex tube latent heat thermal storage system, Journal of Energy Storage, 46 (2022) 103778.

[13] S.S.M. Ajarostaghi, A. Amirsoleymani, M. Arıcı, A. Dolati, L. Amiri, Thermal energy storage with PCMs: A comprehensive study of horizontal shell and multi-tube systems with finned design, Journal of Energy Storage, 72 (2023) 108762.

[14] S.-Z. Tang, H.-Q. Tian, J.-J. Zhou, H. Li, Evaluation and optimization of melting performance in a horizontal thermal energy storage unit with non-uniform fins, Journal of Energy Storage, 33 (2021) 102124.

ACCEPTED MANUSCRIPT

[15] A. Kumar, P. Verma, L. Varshney, An experimental and numerical study on phase change material melting rate enhancement for a horizontal semi-circular shell and tube thermal energy storage system, Journal of Energy Storage, 45 (2022) 103734.
[16] S. Seddegh, X. Wang, A.D. Henderson, A comparative study of thermal behaviour of a horizontal and vertical shell-and-tube energy storage using phase change materials, Applied Thermal Engineering, 93 (2016) 348-358.
[17] X. Yang, Z. Lu, Q. Bai, Q. Zhang, L. Jin, J. Yan, Thermal performance of a shell-and-tube latent heat thermal energy storage unit: Role of annular fins, Applied Energy, 202 (2017) 558-570.
[18] M. Kazemi, M. Hosseini, A. Ranjbar, R. Bahrampoury, Improvement of longitudinal fins configuration in latent heat storage systems, Renewable Energy, 116 (2018) 447-457.
[19] V. Safari, H. Abolghasemi, L. Darvishvand, B. Kamkari, Thermal performance investigation of concentric and eccentric shell and tube heat exchangers with different fin configurations containing phase change material, Journal of Energy Storage, 37 (2021) 102458.
[20] M. Ebrahimnataj Tiji, H.I. Mohammed, R.K. Ibrahem, A. Dulaimi, J.M. Mahdi, H. Sh. Majdi, M.M. Keshtkar, P. Talebizadehsardari, Evaluation of T-shaped fins with a novel layout for improved melting in a triple-tube heat storage system, Frontiers in Energy Research, 10 (2022) 947391.
[21] N.B. Khedher, R.A. Bantan, L. Kolsi, M. Omri, Performance investigation of a vertically configured LHTES via the combination of nano-enhanced PCM and fins: Experimental and numerical approaches, International Communications in Heat and Mass Transfer, 137 (2022) 106246.
[22] D.S. Mehta, K. Solanki, M.K. Rathod, J. Banerjee, Thermal performance of shell and tube latent heat storage unit: Comparative assessment of horizontal and vertical orientation, Journal of Energy Storage, 23 (2019) 344-362.
[23] A. Shahsavar, H.M. Ali, R.B. Mahani, P. Talebizadehsardari, Numerical study of melting and solidification in a wavy double-pipe latent heat thermal energy storage system, Journal of Thermal Analysis and Calorimetry, 141 (2020) 1785-1799.
[24] F.T. Najim, H.I. Mohammed, H.M.T. Al-Najjar, L. Thangavelu, M.Z. Mahmoud, J.M. Mahdi, M.E. Tiji, W. Yaïci, P. Talebizadehsardari, Improved Melting of Latent Heat Storage Using Fin Arrays with Non-Uniform Dimensions and Distinct Patterns, Nanomaterials, 12(3) (2022) 403.
[25] H. Dai, S. Zhou, X. Li, P. Niu, S. He, W. Wang, M. Gao, Charging and discharging performances investigation for a vertical triplex-tube heat exchanger with a tapered configuration and reverse layout, Renewable Energy, (2024) 119976.
[26] N. Zhang, X. Cao, X. Fan, L. Chen, Y. Qu, Thermal storage performance of latent heat thermal energy storage device with helical fin under realistic working conditions, Applied Thermal Engineering, 236 (2024) 121668.
[27] K. Chen, H.I. Mohammed, J.M. Mahdi, A. Rahbari, A. Cairns, P. Talebizadehsardari, Effects of non-uniform fin arrangement and size on the thermal response of a vertical latent heat triple-tube heat exchanger, Journal of Energy Storage, 45 (2022) 103723.
[28] A. Kumar, S.K. Saha, Experimental and numerical study of latent heat thermal energy storage with high porosity metal matrix under intermittent heat loads, Applied Energy, 263 (2020) 114649.
[29] M.A. Basit, S. Dilshad, R. Badar, S.M. Sami ur Rehman, Limitations, challenges, and solution approaches in grid-connected renewable energy systems, International Journal of Energy Research, 44(6) (2020) 4132-4162.
[30] M. Taghilou, F. Talati, Analytical and numerical analysis of PCM solidification inside a rectangular finned container with time-dependent boundary condition, International Journal of Thermal Sciences, 133 (2018) 69-81.
[31] L. Kalapala, J.K. Devanuri, Parametric investigation to assess the melt fraction and melting time for a latent heat storage material based vertical shell and tube heat exchanger, Solar Energy, 193 (2019) 360-371.
[32] L. Pu, S. Zhang, L. Xu, Y. Li, Thermal performance optimization and evaluation of a radial finned shell-and-tube latent heat thermal energy storage unit, Applied Thermal Engineering, 166 (2020) 114753.

[33] A. Brent, V.R. Voller, K. Reid, Enthalpy-porosity technique for modeling convection-diffusion phase change: application to the melting of a pure metal, Numerical Heat Transfer, Part A Applications, 13(3) (1988) 297-318.
[34] S. Mat, A.A. Al-Abidi, K. Sopian, M.Y. Sulaiman, A.T. Mohammad, Enhance heat transfer for PCM melting in triplex tube with internal–external fins, Energy conversion and management, 74 (2013) 223-236.

ACCEPTED MANUSCRIPT